Surface & Coatings Technology 282 (2015) 1–5

Contents lists available at ScienceDirect

Surface & Coatings Technology

journal homepage: www.elsevier.com/locate/surfcoat

Preparation and characterization of osmium films on quartz substrate by magnetron sputtering method

S.L. Li [a], C.Y. Ma [a], Q.Y. Zhang [a,*], X.P. Liu [b], C. Zhang [b], Z. Yi [b]

[a] Key Laboratory of Materials Modification by Laser, Ion and Electron Beams, and School of Physics & Opto-electronic Technology, Dalian University of Technology, Dalian 116024, China
[b] Science and Technology on Reliability and Environmental Engineering Laboratory, Beijing Institute of Spacecraft Environmental Engineering, Beijing 100094, China

ARTICLE INFO

Article history:
Received 11 August 2015
Revised 2 October 2015
Accepted in revised form 6 October 2015
Available online 9 October 2015

Keywords:
Os films
Magnetron sputtering
Mechanical properties
Resistivity

ABSTRACT

Micron-thick osmium films were deposited on quartz substrates with a pulsed −200 V bias using magnetron sputtering method. Application of ~100 nm Ti buffer layer resulted in successful deposition of as thick as ~3 μm Os films. Structure and morphology of the films were studied in terms of X-ray diffraction, scanning electron microscopy and atomic force microscopy, and their dependence on the duty-ratio was revealed. The mechanical properties of the films, namely, the Young's modulus and the hardness, were studied and discussed in comparison with the measurement of Os bulk sample. The Os film was found to be ~40% harder than the bulk sample due to the internal stress and the refined grains. The thickness-dependent resistivity was determined to be $\rho = 13.0 + 1.74/t$ (μΩcm), where t is the film thickness in micron.

© 2015 Elsevier B.V. All rights reserved.

1. Introduction

Osmium (Os) is a special noble metal in the applications of catalysis, fuel cells, electronics, and sensors [1,2]. Os has an as high as 3033 ± 30 °C melting point and a good electrical conductivity (8.1 μΩcm) [2]. At ambient temperature, Os is stable, but easily reacts with atomic oxygen (AO), forming OsO_4 *via* Os + 4O → OsO_4 with a reactions rate of ~3×10^{-26} cm^3 per AO [3]. OsO_4 is volatile, thus Os films have been suggested as a candidate of materials for fabrication of sensors detecting AO in the environment of low earth orbit (LEO, 200–700 km) [3]. However, osmium and rhenium (Re) are the known densest natural elements, with a very low compressibility and a high bulk modulus comparable with that of diamond. Therefore, it is not easy to prepare micron thick Os film on an insulating substrate, such as quartz and ceramics, because the generated high internal stress would make Os films crack or peel during deposition, although the deposition technique and the deposition parameters play a very important role in controlling the residual stresses.

Due to the high melting point, atomic layer deposition (ALD) [1], chemical vapor deposition (CVD) [4–7], microwave-assisted chemical decomposition [8], sol–gel method [9,10], electrodeposition [11–12], and other chemical techniques have been used for deposition of Os films. These chemical methods are capable of preparing submicron Os films, but possess a common problem that the film purity is quite low. The remains such as C and O [4–12] are unfavorable for fabrication of AO sensors. Furthermore, these chemical technologies cannot be applied for deposition of Os films with a thickness meeting the requirements of AO detection in LEO environment. Physical vapor deposition technology, such as electron beam evaporation and magnetron sputtering, enables high-rate deposition of Os films [13], but cracking and peeling are the problems that have to be avoided in fabrication of AO detectors. Li *et al.* [14] had used magnetron sputtering to prepare Os–Ru films on W substrate under a DC negative bias. They found that the films poorly bonded with the substrate, even for the submicron thick films. Therefore, preparation of micron thick Os films with high quality is the key issue for the application of AO detection in LEO environment.

In this study, magnetron sputtering was used to deposit Os films on quartz substrates for the application of AO detection in LEO environment. To improve the film adhesion, a Ti buffer layer was grown on the substrate before deposition of Os films and a pulsed negative bias was applied during film deposition. Using X-ray diffraction (XRD), scanning electron microscopy (SEM), and atomic force microscopy (AFM), we characterized the morphology and structure of the Os films deposited at different duty-ratios of pulsed negative bias. Using a nano-indenter, we studied the mechanical properties of Os films in comparison with Os bulk material. In addition, the dependence of the resistivity on the film thickness was determined.

2. Experimental methods

The deposition of Os films was carried out on a JGP-450 magnetron sputtering system, in which there are three sputtering guns in parallel arrangement for deposition of different materials. 1.5-mm thick fused quartz, which is polished on both sides, was cut into a size of

* Corresponding author.
E-mail address: qyzhang@dlut.edu.cn (Q.Y. Zhang).

http://dx.doi.org/10.1016/j.surfcoat.2015.10.010
0257-8972/© 2015 Elsevier B.V. All rights reserved.

www.spm.com.cn

30 mm × 20 mm for Os film deposition. The substrates were successively cleaned in acetone, ethanol, deionized water and finally dried through nitrogen stream, and then rapidly loaded into the vacuum chamber. The target for deposition of Os films was prepared by powder metallurgy protected in pure Ar ambient using 99.99% Os powder. The target purity for deposition of the Ti buffer layer is 99.99%. The Ti buffer layer and Os films were deposited at 550 °C using 99.999% Ar as the working gas under the pressures of 0.5 and 1.8 Pa, respectively. Before deposition, the base pressure was pumped to be better than 5×10^{-4} Pa using a turbo-molecular pump backed by rotary pump. Prior to the film deposition, the Ti and Os targets were pre-sputtered for 10 min to remove any surface contamination. Ti and Os targets were driven by an 80 W radio-frequency and a 120 W DC powers, respectively. The deposition time for the Ti buffer layer was 15 min, and the Os films with different thickness were deposited by controlling the deposition time. During the deposition of Ti buffer layers and Os films, a pulsed −200 V bias with a 35 kHz repeating frequency was applied to the sample holder. To study the role of the pulsed negative bias, the duty-ratio was set to 0%, 5%, 10%, 15% and 20%, respectively. After deposition, the samples were slowly cooled to 400 °C in a ~2 °C/min rate. After preservation for 1 h at 400 °C, the temperature was decreased below 100 °C in an average cooling rate of ~1.5 °C/min.

The Os films were analyzed by XRD on Bruker D8 DISCOVER using a Cu K_{α} radiation aligned by a göbel mirror, which provides a ~0.03° divergence for the X-ray beam. Coupled scan in ω–2θ mode is used for collection of XRD patterns with 0.02° intervals. MTS Nano-Indenter XP was used to characterize the hardness and elastic modulus of the films with different thickness. AFM (Benyuan CSPM5000) and SEM (Hitachi S-4800) were used to observe the surface and cross-sectional morphology of Os films. The film compositions were determined by X-ray energy dispersive (EDX) spectroscopy. The film thickness was basically determined by the weighting method and checked by the cross-sectional SEM observation. The measurement of Os film resistance was performed on a RTS-9 four-probe testing instrument and 12 points were measured for each sample, and then the deviation in the film resistivity was determined.

3. Results and discussion

3.1. Morphology and structure of the Os films

Fig. 1 shows the typical in-plane and cross-sectional SEM images of the Os film grown on the quartz substrate, which was deposited at a pulsed −200 V bias with a 15% duty-ratio. The Os film exhibits a smooth surface and a dense column structure with ~3.3 μm thickness. Between the Os film and the quartz substrate, there is a ~100 nm Ti buffer layer, with which the Os film is well adhered to the quartz substrate without cracking or peeling. EDX analysis showed that Os is the only element that could be detected above noise level, indicating the high purity of the Os films, as shown in the inset of Fig. 1(a). The above results revealed that high-quality micron-thick Os films have been successfully deposited on the quartz substrate using magnetron sputtering method under the pulsed negative bias.

To study the role of biasing pulses in the deposition of Os films, the duty-ratio of the pulsed negative bias was set to 0, 5, 10, 15, and 20%, respectively. Fig. 2 shows the AFM images, which are in accordance with the in-plane SEM observation, of Os films deposited at different duty-ratios. The Os films deposited at low duty-ratios of the pulsed negative bias exhibit island-like morphology. With the increase in the duty-ratio, the island-like morphology gradually disappers, indicating enhancement of ion bombardment producing the smooth surface. Fig. 2(f) depicts the dependence of the surface roughness on the duty-ratio of the pulsed negative bias. Of the films deposited at the duty-ratios below 5%, the surface roughness is ~3.7 nm. With increasing the duty-ratio from 10% to 20%, the surface roughness linearly decreases from ~1.5 nm to a value less than 1 nm, which can be ascribed to the smoothing effect of ion bombardment. Measurement showed that the deposition rate is not obviously changed when increasing the duty-ratio from 0% to 20%.

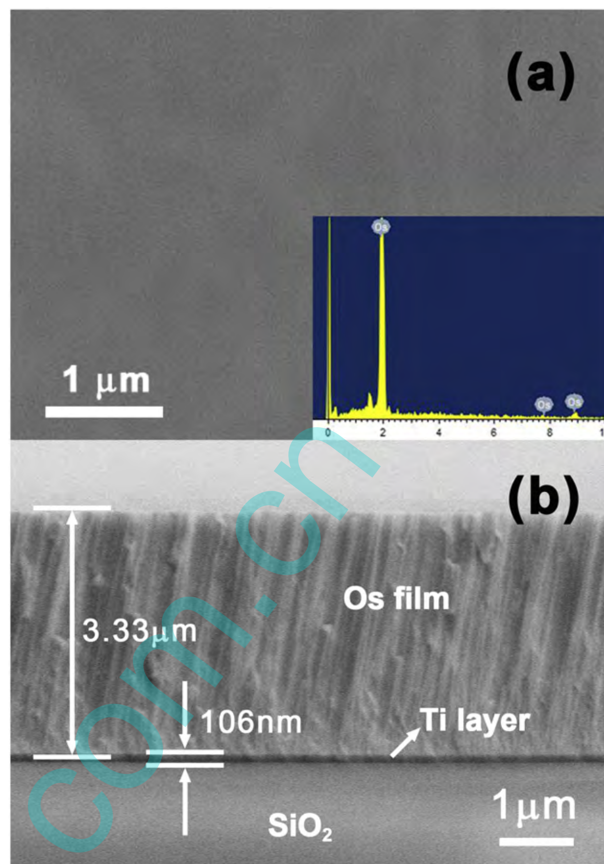

Fig. 1. Typical in-plane (a) and cross-sectional (b) SEM image of Os film on quartz substrate. The inset is the EDX spectrum of the Os film.

Fig. 3 shows the XRD patterns of Os films deposited at the given duty-ratios in the same deposition time. For comparison, a standard PDF card (87-0716 for a hexagonal phase with $P6_3/mmc$ space group) is also present. Compared to the standard intensities of Os powder, the Os films are textured mainly in the (001) or (100) direction. For the films deposited at the duty-ratios below 15%, the film growth prefers to the (001) direction. For the film deposited at the duty-ratio of 20%, the preferential orientation changes to be (100). Similar change in preferential orientation was also observed by Li *et al.* [14] in the deposition of Os–Ru films when increasing bias power, being consistent with our conclusions. The dependence of preferential orientation on ion bombardment is a complicated problem related to the nucleation thermodynamics. In short, ion bombardment usually promotes formation of nuclei due to creation of defects, and then increasing the density of critical nuclei, but reducing their sizes. The change in grain size affects the stability of the critical nuclei, which is related to the surface free energy of grains and dominates the preferential orientation of grains. We must emphasize here that the critical size of grains in the nucleation stage differs from the grain size in the film because of the coalescence between grains during growth. In general, the grain size increases with the increase in film thickness when the film thickness is lower than a certain value.

The grain sizes in the films deposited at different duty-ratios were estimated by Scherrer method using the full width at half maximum (FWHM) of the diffraction peaks. We found that the duty-ratio has no significant effect on the grain size, except for the (100) textured film deposited at 20% duty-ratio, as shown in Fig. 4. The grain sizes in the (001) textured films deposited at different duty-ratios are approximately

www.spm.com.cn

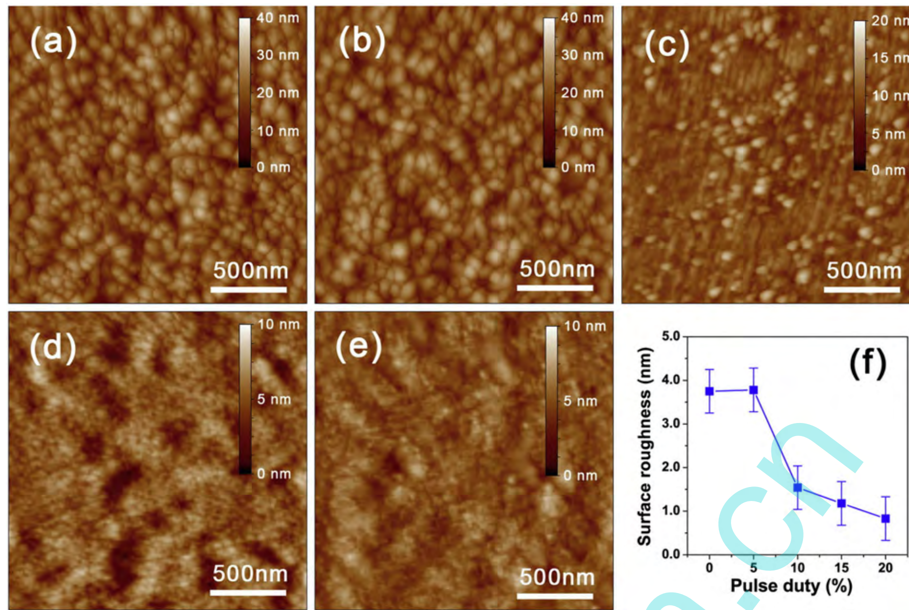

Fig. 2. (a–e) AFM images of the Os films deposited at the duty-ratios of 0, 5, 10, 15, and 20%, (f) surface roughness of the film plotted as a function of the duty-ratio.

equal. To preclude the influence of strains on the determination of grain size, Williamson–Hall method was used to correct the grain size using the strains calculated by the lattice parameters. The corrected gain sizes in the (001) textured films are 54.0 ± 1.4 nm. Therefore, we conclude that the growth temperature is the crucial factor determining the grain size in the films while the pulsed negative bias affects the growth orientation and the surface roughness.

In comparison with the standard PDF card, we found the diffraction peaks shifting to the low angles, indicating the films suffering a compressive stress, which might be created by the difference between the thermal expansion coefficients of Os and quartz substrate [15,16]. Using the Young's modulus (648 GPa) and Poisson ratio (0.233) of metal Os [17], the internal stress in the Os films was estimated to decrease from 8 to 1.5 GPa with the increase in the duty-ratio of pulsed negative bias, as shown in Fig. 4. We must point out that the modulus varies in the range between the upper and the lower limits for a polycrystalline material, depending on its degree of texturization. The upper limit is the Voigt bound [18], which is the average based on an assumption of uniform strain, and the lower limit is the Reuss bound [19], which is obtained by assuming a uniform stress. The effective modulus of a polycrystalline material is usually estimated by the arithmetic average of Voigt and Reuss bounds under the Voigt–Reuss–Hill approximations [20]. Therefore, the stress calculated by the Young's modulus is an estimation for the textured Os films, instead of the true values. Despite the uncertainty, the estimation can be used as a measure evaluating the stresses in the films. The dependence of internal stress on the duty-ratio of pulsed negative bias is quite abnormal because ion

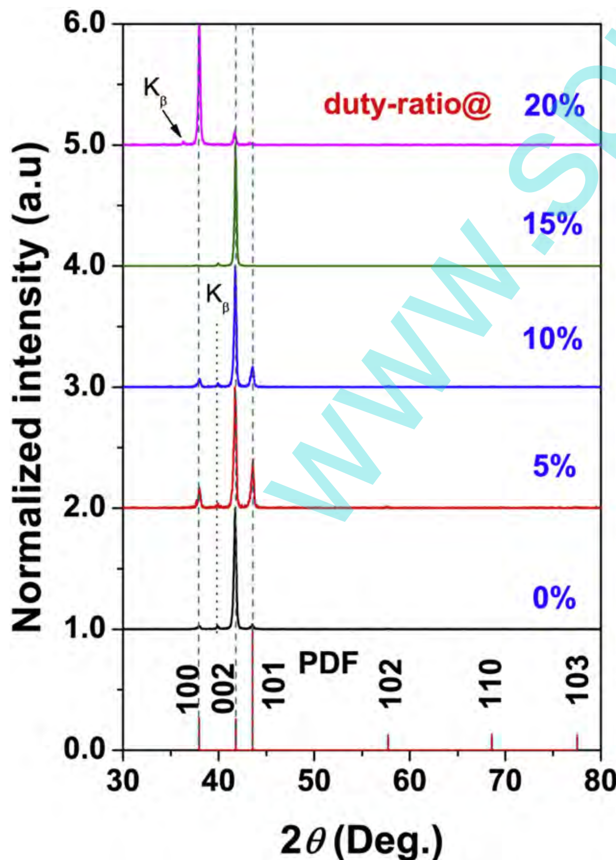

Fig. 3. XRD patterns of the Os films deposited at the given duty-ratios of the pulsed bias. XRD data from PDF card (87–0716) is present for comparison.

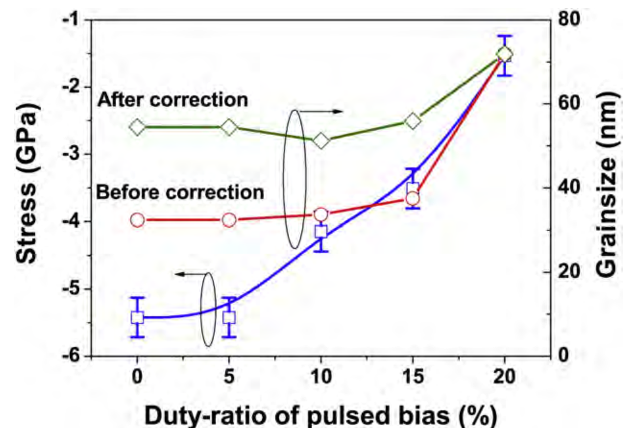

Fig. 4. Internal stresses and grain sizes of the Os films plotted as a function of the duty-ratio of the pulsed negative bias.

www.spm.com.cn

bombardment usually produces increase in the film density, thus a higher stress is expected with the increase in the duty-ratio of pulsed negative bias. However, the stress is decreasing with the increase in the duty-ratio of pulsed negative bias, indicating that the ion bombardment produces a release of internal stress in the Os films. Though we do not know the mechanism releasing the internal stress in Os films, our results show that ion bombardment is capable of preventing the Os films from cracking or peeling. On the other hand, we found that a slow decrease in temperature after deposition is necessary for preventing the films against cracking or peeling out.

3.2. Mechanical properties of the Os films

Due to the high elastic modulus, Os is predicted to possess a high hardness. For example, Os' hardness was estimated to be as high as ~40 GPa [21] using a linear response theory of hardness on shear modulus or Young modulus, but the relevant experimental data is unavailable in literature. Therefore, the mechanical properties of Os' bulk material, which was prepared by powder metallurgy, were measured, as shown in Fig. 5(a). The displacement-dependent curves of Young's modulus and hardness showed that the mechanical variables, both of the Young's modulus (Y) and hardness (H), reach to their saturation when the indentation depth goes over 200 nm, but slightly decrease due to overload when the indentation depth (d) exceeds ~600 nm. Thus, the data in the range of 300–500 nm were used for calculation of their averages. The average of Young's modulus is $Y = 634.6 \pm 41.5$ GPa, very close to 648 GPa reported in literature [17], but the hardness $H = 16.4 \pm 1.9$ GPa, only ~40% of that predicted by the linear response theory. As a matter of fact, this hardness is an extremely high value for a metal material because it is comparable with many metal nitrides [22–30], such as TiN (20–30 GPa), ZrN (17–21 GPa), TaN (16–20 GPa) and CrN (25–31 GPa).

The mechanical properties of Os films differ from the bulk material. The Os films exhibit the mechanical properties depending on the film thickness due to the substrate effect. Fig. 5(b) shows the displacement-dependent mechanical responses of a ~3 μm thick Os film. A maximum value of Young's modulus can be taken at the indentation depth of ~30 nm, $Y = 620.3 \pm 133.6$ GPa, which is close to, but slightly lower than that of the bulk material. With the increase in displacement, the modulus value declines rapidly, suggesting the measurement does not achieve to the saturation due to the substrate effect. If the

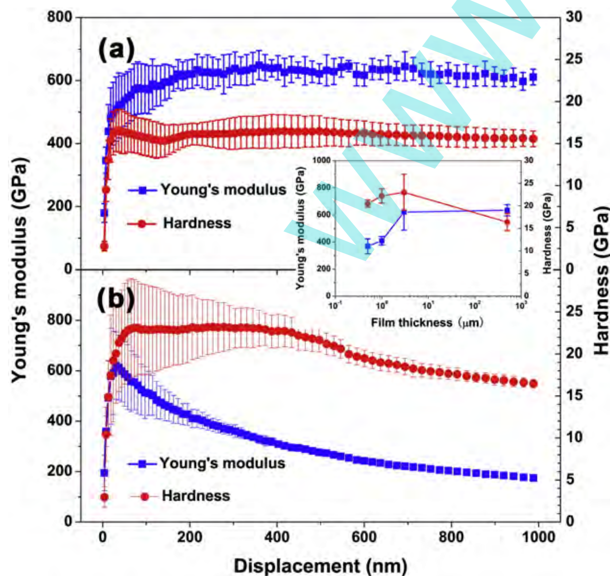

Fig. 5. Dependence of Young's modulus and hardness on indentation depth, (a) Os bulk material, (b) ~3 μm thick Os film. The inset shows the measured Young's modulus and hardness plotted as a function of the film thickness.

maximum Y value can be used as a measure evaluating the Young's modulus of the Os film, we found that this value decreases with the decrease in film thickness, as shown in the inset of the figure. As a matter of fact, films usually exhibit a larger Young's modulus than the bulk materials because of the existence of residual stress in the films, thus the measured Young's moduli are indeed lower than the true values of the Os films. The hardness measurement differs from the Young's modulus that a platform appears in the indentation depth range of 60–360 nm, which can be used for calculation of the film hardness. The average in this depth range is $H = 23.0 \pm 4.0$ GPa, ~40% higher than that of the bulk material, indicating that the Os films have a high hardness comparable with TiN, ZrN or other superhard coatings. Despite the substrate effects, we could obtain a relatively high value, even for the film with ~500 nm thickness, which presents a platform in the indentation depth range of 30–50 nm when a high-resolution displacement is used. As shown in the inset, the films with different thicknesses exhibit a hardness higher than that of the bulk material, thus we ascribe the enhancement of film hardness to the internal stress and the refined grains in the films. As the measured Young's moduli cannot represent the true values of the Os films, we estimated the film moduli using the equation $B = B_0 + B'P$, where B_0 is the bulk elastic modulus of Os metal, P is the hydrostatic pressure, and B' is the pressure parameter of linear response. For Os films, $B_0 = 405$ GPa [17] and P is replaced by the internal stress (~3.5 GPa) estimated by XRD analysis. The pressure parameter B' is related to the Grüneisen parameter γ by $B' = \frac{dB}{dP} = 2\gamma + 1$, $\gamma = 2.22$ for Os [17]. Therefore, the bulk elastic modulus was estimated to increase by ~5% (19 GPa) in comparison with the bulk material. As a consequence, the contribution of grain size in the film to the hardness can be estimated by $H/1.05 \approx 1.33\,H_0$, where H_0 is the hardness of bulk material. Therefore, we conclude that the refined grains in the Os films contribute to the enhancement of film hardness by ~33%.

3.3. Electrical properties of Os films

The film resistivity is a crucial parameter for detecting AO dose in LEO environment. However, the film resistivity is usually a function of film thickness, thus we studied the dependence of the resistivity on the thickness of the films, which were deposited at the 15% duty-ratio of the pulsed negative bias because these samples exhibit the best resistance against oxygen corrosion. The film thickness was determined by the weighting method and checked by the cross-sectional SEM images. Fig. 6 depicts the resistivity plotted as a function of the film thickness, which are the averages over the data measured at 12 points. The deviation of the film resistivity is within 5.5%, indicating a good uniformity in the film thickness. The dependence of the resistivity (ρ) on the film thickness can be fitted by $\rho = 13.0 + 1.74/t$ (μΩcm), where t is the film thickness in μm. Because the film thickness is much larger than

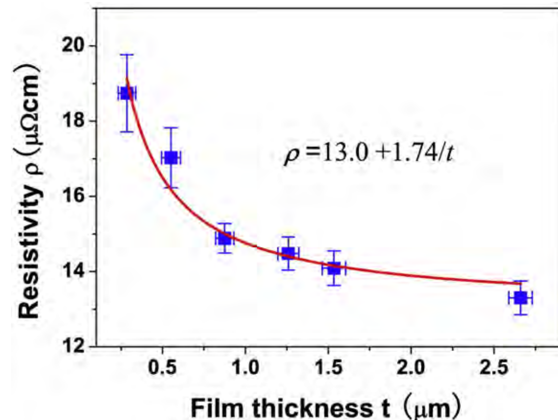

Fig. 6. Resistivity plotted as a function of film thickness.

www.spm.com.cn

the electron free path in metal, the scattering of electrons at the surface and at the interface between the film and substrate is unimportant. Therefore, the resistance is primarily determined by the scattering of electrons by the lattice (phonons) and defects (impurity, grainboundary, dislocation, *etc*) in the films. The scattering of electrons by the lattice and defects are related to the temperature and the defect density, respectively. The thickness-dependent resistivity, therefore, is an indication that the defect density in the Os films gradually decreases with the increase in the film thickness, being consistent with our XRD measurement for the FWHMs of (100) and (002) diffraction peaks. The resistivity for $t \rightarrow \infty$ is $\rho_0 = 13.0$ μΩcm, ~60% higher than that of bulk material (8.1 μΩcm) [2], indicating that the Os films are of high-quality, but the defect density in the Os films is quite large in comparison with the bulk material prepared by the metallurgical method.

4. Conclusions

A pulsed negative biasing magnetron sputtering was used to deposit micron-thick Os films on quartz substrates using a ~100 nm Ti buffer layer. As thick as ~3 μm Os films were successfully prepared and exhibited high purity and good adhesion to the substrate. XRD analysis revealed that the films are textured and the preferential orientation depends on the duty-ratio of the pulsed negative bias. With increasing the duty-ratio from 0% to 20%, the preferential orientation of the textured films changes from (001) to (100) and the surface roughness decreases from 3.7 nm to a value less than 1 nm. The grain size in the films is mainly determined by the growth temperature, leading to 54.0 ± 1.4 nm in average for the (001) textured films deposited at different duty-ratios of negative pulsed discharge. The film hardness is ~40% higher than that of bulk material. The contributions of the thermal stress and refined grains in the films to the hardness enhancement were estimated to be ~5% and ~33%, respectively. The dependence of resistivity on the film thickness was determined to be $\rho = 13.0 + 1.74/t$ (μΩcm), where t is the film thickness in μm.

References

[1] J. Hämäläinen, T. Sajavaara, E. Puukilainen, M. Ritala, M. Leskelä, Chem. Mater. 24 (2011) 55.
[2] W.M. Haynes (Ed.), *CRC Handbook of Chemistry and Physics*, 91st ed.CRC Press/Taylor and Francis, Boca Raton, FL, 2011 (Internet Version 2011).
[3] X.P. Liu, J.Y. Tong, S.H. Xiang, Z. Jia, Spacecraft Environ. Eng. 27 (3) (2010) 300.
[4] Y. Chi, H.L. Yu, W.L. Ching, C.-S. Liu, Y.-L. Chen, T.-Y. Chou, S.-M. Peng, G.-H. Lee, J. Mater. Chem. 12 (2002) 1363.
[5] Y. Senzaki, W.L. Gladfelter, F.B. McCormick, Chem. Mater. 5 (1993) 1715.
[6] H.L. Yu, Y. Chi, C.S. Liu, S.-M. Peng, G.-H. Lee, Chem. Vap. Depos. 7 (2001) 245.
[7] E.P. Boyd, D.R. Ketchum, H. Deng, S.G. Shore, Chem. Mater. 9 (1997) 1154.
[8] E. Borja-Arco, O. Jiménez-Sandoval, J. Escalante-García, L. Magallón-Cacho, P.J. Sebastian, Int. J. Electrochem. 2011 (2011) 1.
[9] F. Quaranta, R. Rella, P. Siciliano, S. Capone, M. Epifani, L. Vasanelli, A. Licciulli, A. Zocco, Sensors Actuators B 58 (1999) 350.
[10] M. Epifani, A. Forleo, S. Capone, F. Quaranta, R. Rella, P. Siciliano, L. Vasanelli, IEEE Sensors J. 3 (2003) 827.
[11] T. Jones, Met. Finish. 100 (2002) 84.
[12] A. Ignaszak, E. Gyenge, Electrochim. Acta 95 (2013) 268.
[13] D. Josell, C. Witt, T.P. Moffat, Electrochem. Solid-State Lett. 9 (2006) C41.
[14] W.C. Li, S. Roberts, T.J. Balk, IEEE Trans. Electron Dev. 56 (2009) 805.
[15] J. Oishi, T. Kimura, Metrologia 5 (1969) 50.
[16] J.W. Arblaster, Platinum Metals Rev. 57 (2013) 177.
[17] C. Pantea, I. Stroe, H. Ledbetter, J.B. Betts, Y. Zhao, L.L. Daemen, H. Cynn, A. Migliori, Phys. Rev. B 80 (2009), 024112.
[18] W. Voigt, Lehrburch der Kristallphysik, Teubner, Leipzig, 1928.
[19] A. Reuss, Z. Angew. Math. Mech. 9 (1929) 49.
[20] R. Hill, Proc. Phys. Soc. Lond. 65 (1952) 350.
[21] A.L. Ivanovskii, Inorg. Mater. Appl. Res. 3 (2012) 319.
[22] Q.Y. Zhang, X.X. Mei, D.Z. Yang, F.X. Chen, T.C. Ma, Y.M. Wang, F.N. Teng, Nucl. Instr. Methods B 127 (128) (1997) 664.
[23] Q.Y. Zhang, Z.H. Long, C.S. Ren, B.H. Guo, T.C. Ma, Surf. Coat. Technol. 103-104 (1998) 195.
[24] T. Zhang, X. Wang, Acta Mech. Sinica 35 (2003) 498.
[25] Z.G. Xiao, T.D. Mantei, Surf. Coat. Technol. 177 (2004) 389.
[26] J. An, Q.Y. Zhang, Surf. Coat. Technol. 200 (2005) 2451.
[27] X.M. Xu, J. Wang, Y. Zhao, Q.Y. Zhang, Phys. Sin. 55 (2006) 5380.
[28] X.M. Xu, J. Wang, J. An, Y. Zhao, Q.Y. Zhang, Surf. Coat. Technol. 201 (2007) 5282.
[29] J. An, Q.Y. Zhang, Structure, Mater. Charact. 58 (2007) 439.
[30] M.A. Auger, J.J. Araiza, C. Falcony, O. Sanchez, J.M. Albella, Vacuum 81 (2007) 1462.

www.spm.com.cn